Ionics (2022) 28:4817–4824
https://doi.org/10.1007/s11581-022-04723-z

ORIGINAL PAPER

Chemically dezincified copper nanowires catalysts with competitive selectivity for ethylene production by carbon dioxide reduction reaction

Shiji Zhang[1] · Rui Zhang[1] · Yilin Yao[1] · Xin Zong[1] · Jinqiu Zhang[1] · Yueping Xiong[1] · Peixia Yang[1] · Maozhong An[1]

Received: 30 May 2022 / Revised: 6 August 2022 / Accepted: 15 August 2022 / Published online: 19 August 2022

Abstract

Electrochemical reduction of carbon dioxide is an attractive and challenging strategy to solve the problems of renewable energy storage and carbon neutral. However, activity, selectivity, and stability of present developing catalysts for production of C_2H_4 are not as high as required for practical applications. Herein, we report dezincified copper nanowires (pre-CuZn-CuNW) derived from an electrodeposited CuZn alloy by a wet chemical method for electrochemical reduction of carbon dioxide to C_2H_4. Compared with pre-Cu-CuNW (the copper nanowires derived from a bulk Cu), the pre-CuZn-CuNW significantly enhances the catalytic activity and the selectivity for C_2H_4. The partial normalized current density of the pre-CuZn-CuNW for production of C_2H_4 increases to 183 mA•cm^{-2}, which is about twice relative to pre-Cu-CuNW. The faradaic efficiency (FE) of the pre-CuZn-CuNW for C_2H_4 can be maintained over 46% for 24 h during carbon dioxide reduction reaction. The improved catalytic performance can be attributed to the formation of a special nanowire structure with larger electrochemical active surface area and higher intrinsic activity of the pre-CuZn-CuNW during the dealloying process.

Keywords Copper nanowires · Chemical dezincification · Electrodeposition · CuZn alloy · Ethylene

Introduction

In recent years, under the theme of the era of carbon neutrality, more people have focused on energy and environmental problems caused by carbon dioxide [1]. Electrochemical reduction is also considered as the most effective CO_2 conversion method [2–4]. It is worth mentioning that Berlingette and his research team [5] optimized the carbon dioxide reduction reaction (CO_2RR) platform to improve the transmission of carbon dioxide in the H-type electrolytic cell, increasing the current density. Many metal catalysts have been used to study the reduction of CO_2. Because of the wide application of ethylene (C_2H_4) and ethanol (C_2H_5OH) in industry, metal copper has good selectivity to C_{2+} products [6, 7], which makes the research on highly selective copper metal catalyst more meaningful [8].

Researchers focus on developing different nano-copper catalysts to improve the selectivity for C_2H_4 production [9–11]. Among them, oxide-derived copper (OD-Cu) has been extensively studied due to its excellent reduction of CO_2 to C_2 products [12]. Many factors are widely believed to cause the special properties of OD-Cu, such as higher grain boundary density [13], single crystal plane orientation [14], stronger local pH [8, 15], and product reabsorption [16]. When copper oxide derivatives prepared on copper foam was used as the substrate, the faradaic efficiency (FE) for C_{2+} production reached 70% [17]. The copper nanowire catalyst prepared on a copper mesh substrate was used for electrocatalytic reduction of CO_2 at a lower overpotential [18]. Catalysts grown on these substrates lack hydrophobic permeability and cannot be used directly in flow cells. Although the use of Nafion plasma binder to prepare gas diffusion electrodes can greatly improve the current efficiency of the electroreduction reaction [19], the preparation process is complicated and some active centers of the catalyst are covered.

As one of the simple and controllable material preparation methods, electrodeposition can be used to prepare catalysts with various composition and micromorphology

✉ Jinqiu Zhang
zhangjinqiu@hit.edu.cn

[1] MIIT Laboratory of Critical Materials Technology for New Energy Conversion and Storage, School of Chemistry and Chemical Engineering, Harbin Institute of Technology, Harbin 150001, People's Republic of China

by adjusting electrolytes, applying potential, electrodeposition methods, etc. Pardal et al. performed a series of experiments to study the electrodeposition of copper for the electrochemical conversion of CO_2 to C_2 products [20]. By changing the concentration of H_2SO_4, the hydrogen evolution reaction was intensified, and the adhesion of hydrogen bubbles was promoted, resulting in the accumulation of copper particles around the bubbles to form a honeycomb surface. The current efficiency for C_2H_4 production increased significantly from around 7 to 15%. The electrolyte with 3,5-diamino-1,2,4-triazole (DAT) as an additive can be used to electrodeposit porous copper films, which retarded the deposition rate of copper and promoted the formation of copper catalysts with high surface area [21]. In this case, the FE for C_2H_4 production reached over 60% at − 0.5 V (vs RHE, same as below). Ryting et al. prepared Cu-Pd bimetallic catalysts on carbon paper (CP) by dynamic hydrogen bubble template electrodeposition. In an H-type electrolyzer, the FE for C_2H_4 production could reach 45.2% at − 1.2 V and the current density was 17.4 mA•cm^{-2} [22].

Herein, we report a gas diffusion electrode (GDE) composed of dezincified copper nanowires (pre-CuZn-CuNW) derived from an electrodeposited CuZn alloy. 5,5-dimethylhydantoin (DMH) is applied as a complexing agent in the electrolyte for directly electrodeposition of the CuZn alloy on the carbon paper. The formation of nanowires and the dezincification of alloy are proceeded in one-step that is dipping in an alkaline solution. The catalytic performances of dezincified Cu nanowires for electroreduction CO_2 are studied in a flow cell. Electrochemical measurements demonstrate that the catalyst has excellent C_2H_4 selectivity with high activity and stability due to the increased electrochemical active surface area and intrinsic activity resulted by chemical dezincification.

Experimental

Materials and methods

Carbon paper and Fuma FAA-PK-130 anion exchange membrane were purchased from Toray Industries and Gaoss Union, respectively. Deionized water was produced using a Millipore system and used throughout. All chemicals were analytical-grade reagents and used without further purification.

The micromorphologies of catalysts were characterized via scanning electron micrographs (SEM) recorded by using a ZEISS system (SUPRA55010102) and transmission electron microscopy (TEM, JEM 2100, 200 kV). X-ray diffraction (XRD, D/max2550V with Cu Kα radiation of $\lambda = 1.541841$ Å) was used to determine the crystal structures. X-ray photoelectron spectroscopy (XPS) experiments were applied on an AXIS ULTRA DLD spectrometer to analyze elemental contents.

Cyclic voltammetry (CV), linear sweep voltammetry (LSV), and amperometric current–time (*i-t*) curve measurements were measured by an electrochemical workstation (CHI660E). A 0.1 M $KClO_4$ was used in a H-type cell for the measurement of CV at various scan rates, 1 M KOH solution in N_2 or CO_2 saturated was used in a flow cell for the measurement of LSV at 20 mV•s^{-1}, and 1 M KOH solution in CO_2 saturated was used in a flow cell for the measurement of *i-t* curve. The GDE prepared in this work, a platinum electrode, and Ag/AgCl were used as the working electrode, the counter electrode, and the reference electrode, respectively. The value of the potential versus Ag/AgCl was converted to the reversible hydrogen electrode (RHE) scale using the Eq. (1):

$$E(V \text{ vs RHE}) = E(V \text{ vs Ag/AgCl (3 M KCl)}) + 0.21 \text{ V} + 0.059 \text{ pH} \quad (1)$$

The CV curves were applied for measurement of electrochemical active surface area (ECSA). There is a proportional relationship between ECSA and electric double layer capacitance (C_{dl}), as shown in Eq. (2). C_s is usually located between 20–60 μF•cm^{-2}, and 60 μF•cm^{-2} is used in this paper [23]. In the case of comparing ECSA of catalysts composed by same metal, the value of C_{dl} can be used to evaluate the order of the ECSA of the catalyst because C_s is a constant.

$$ECSA = C_{dl}/C_s \quad (2)$$

Since the CV curves were measured in the voltage range without oxidation–reduction reaction, the potential scanning range is relatively small, and the electric double-layer capacitance remains approximately unchanged. At this time, the relationship between the non-faradaic current (i_c) and the scanning rate is shown in Eq. (3). Here, i_c is electric double-layer current (the difference between the cathode current and the anode current from the CV curve). When the scanning rate is plotted with the i_c, a straight line is obtained. The slope of the line is the electric double-layer capacitance (C_{dl}).

$$i_c = C_{dl}\frac{d\varphi}{dt} \quad (3)$$

Preparation of copper nanowires

The preparation process of the GDE loaded with copper nanowires catalyst is shown in Fig. 1. CuZn alloy was electrodeposited on a piece of hydrophobic carbon paper from an electrolyte containing copper sulfate, zinc sulfate, DMH, and potassium citrate, as Supplementary S1.1 and Table S1

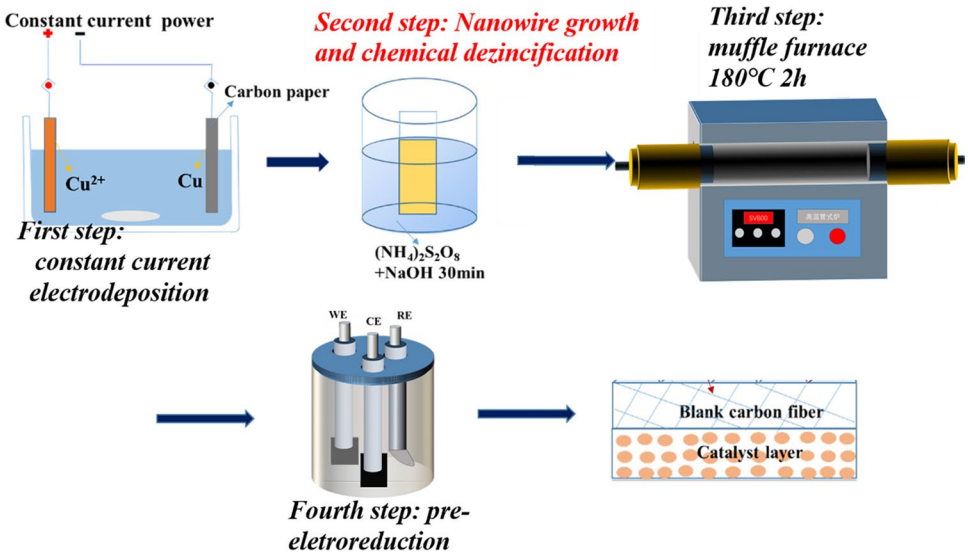

Fig. 1 Schematic illustration of procedure for preparing Cu nanowires on carbon paper as GDEs

introduce. In the pre-experiment, three different complexing agent systems were compared. The copper nanowire catalyst derived from copper in the electrodeposition system with DMH as the complexing agent has better catalytic properties (Fig. S1), so the electrodeposition of CuZn alloy was carried out in the DMH system.

Borrowed the wet chemical oxidation method for growing copper hydroxide nanowires on copper foil [11], chemically dezincified $Cu(OH)_2$ nanowires on carbon paper were obtained in one step by dipping the electrodeposited sample into the solution composing by NaOH and $(NH_4)_2S_2O_8$. By an annealing process with high-temperature sintering (Supplementary S1.2), $Cu(OH)_2$ nanowires turn to CuO nanowires. The next step is to obtained Cu nanowires (pre-CuZn-CuNW) on the carbon paper under a constant electrochemical reductive potential for applying as the GDE of the flow cell (Supplementary S1.3).

In order to explore the role of zinc in the precursor CuZn alloy, Cu was electrodeposited on the carbon paper and copper nanowires (pre-Cu-CuNW) were prepared for comparison in the same steps as Fig. 1 shown, for comparison with CuZn alloy and its derived copper nanowires (pre-CuZn-CuNW).

CO_2 reduction electrolysis and product analysis

A flow cell (purchased from Gaoss Union Photoelectric technology co. LTD) was used in the experiment, including a cathode chamber, an anode chamber, and a CO_2 gas chamber. The anion exchange membrane was used to separate the cathode and anode to prevent cathodic liquid products from flowing into the anode chamber and to ensure the transmission of hydrixude ion transmission.

Both cathode and anode chambers had a precisely machined window (12.5 mm × 8 mm), so the geometric area of the working electrode was 1 cm^2. The working electrode was a GDE that prepared as "Materials and methods" shown. For a GDE, one side of carbon nanofibers (Fig. S2a) was covered by the catalyst, while carbon black and polytetrafluoroethene (PTFE) were loaded on the other side in the factory (Fig. S2b). It means that the carbon black on the back side of the catalyst provided a thin gas diffusion layer to transmit carbon dioxide to the catalyst surface. The presence of PTFE prevented the catholyte from immersing the catalyst and kept the hydrophobicity of the GDE. Thus, a GDE provided three-phase interfaces for CO_2 reduction reaction taking place. The concentration (C) of cathodic gas products, such as ethylene, carbon monoxide, and hydrogen, was detected by gas chromatography (GC) and the FE of a specific product was calculated by Eq. (4):

$$FE = nFCvp \,/\, jRT \tag{4}$$

where n is the number of electrons transferred to produce one molecule of a product, F is the Faraday's constant (96,500 C•mol^{-1}), C is the concentration of a product determined by GC (at%), v is the flow rate (0.5 ml·s^{-1}) of CO_2 bubbled into the electrolyte, P and T are the pressure (101,325 Pa) and temperature (298 K) of the gas sampled by the GC sample loop, respectively, j is the total current when sampling, and R is the gas constant (8.314 J·mol^{-1}·K^{-1}).

Results and discussion

Formation and characterization of copper nanowires derived from CuZn alloy

CuZn alloy was successfully electrodeposited on the carbon paper. From EDS elemental maps (Fig. S3), Zn is uniformly

distributed on the carbon fibers. Figure 2a shows the XRD patterns of Cu, CuZn alloy, pre-Cu-CuNW, and pre-CuZn-CuNW on GDEs. The three groups of peaks at 43.3°, 50.4°, and 74.1° correspond to (111), (200), and (220) of Cu, and peaks appearing in 26.6° can be indexed to carbon. Compared with Cu, it is noticeable that the peak near 43° of CuZn pattern shifts leftwards. The peak shift is believed to be caused by the formation of CuZn alloy during electrodeposition. The intercalation of Zn into the Cu crystal lattice leads to an increase in the interplanar spacing of Cu and causes lattice distortion [24]. Therefore, it can be confirmed that CuZn alloy is obtained by the electrodeposition.

The success of chemical dezincification requires quantitative analysis of the relative content of Zn before and after the reaction, so XPS measurement was used to verify the change of the relative content of Zn on the surface of the catalyst. The carbon element rich in the GDE can be used as a reference for comparing the content of Zn before and after the reaction. By measuring the relative contents of Zn and C in CuZn alloy and pre-CuZn-CuNW, the Zn atomic content is significantly reduced from 2.99 to 0.52% (Fig. 2b and c), which is consistent with the conclusion in literature [24] that chemical dezincification achieves dealloying. Figure 2d shows the XPS pattern of Zn 2p of pre-CuZn-CuNW. The characteristic peaks with binding energies of 1022.3 eV and 1045.3 eV correspond to the Zn 2p3/2 and Zn 2p1/2 regions. The characteristic peaks corresponding to Zn in the pre-CuZn-CuNW were not observed, which further indicated that the method of chemical dezincification successfully reduced the content of Zn in the catalyst. After the process of chemical dezincification, the left shift around 43° even occurs in the XRD spectrum, which can be explained by the fact that the vacancies left by the entry and exit of zinc atoms are still existing [24]. Zhang et al. found that the vacancies caused by zinc atoms would result in a special porous structure of catalysts with a large surface area [25].

The surface morphologies of pre-CuZn-CuNW were investigated by SEM and TEM. Compared with CuZn alloy (Fig. 3a), pre-CuZn-CuNW (Fig. 3b) has abundant nanowires and presents a radial structure. This special nanowire structure benefits from the use of NaOH and $(NH_4)_2S_2O_8$ in the second step, enabling the growth of nanowires at the same time as chemical dezincification. The diameter of pre-CuZn-NW is around 170 nm, which can be determined by TEM (Fig. 3c). The EDS elemental maps show the elemental distribution in the pre-CuZn-CuNW, including Cu, Zn, C, and O, as shown in Fig. 3d–g. The presence of Zn element is consistent with the XPS analysis of pre-CuZn-CuNW. The SEM images of bulk Cu and its derived pre-Cu-CuNW are shown in Fig. S4, while the distribution of the copper nanowires is not as regularly radial as that of pre-CuZn-CuNW.

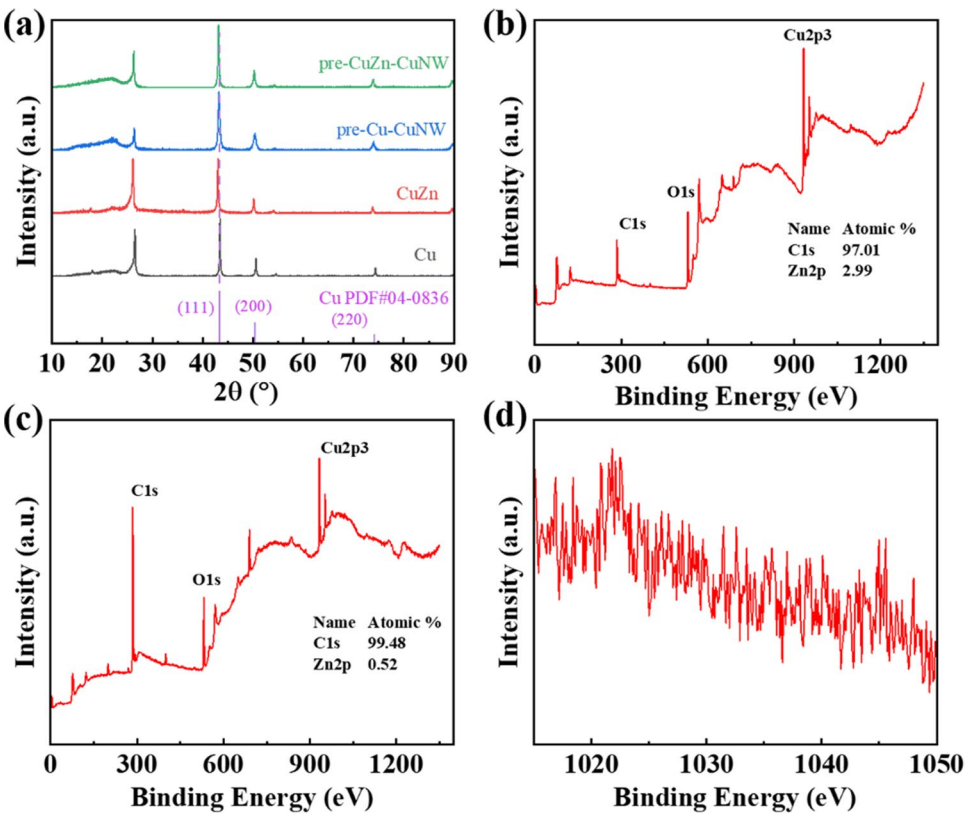

Fig. 2 **a** XRD patterns of the bulk Cu, CuZn alloy, pre-Cu-CuNW, and pre-CuZn-CuNW; **b** XPS pattern of CuZn alloy; **c** XPS pattern of pre-CuZn-CuNW; and **d** XPS pattern of Zn 2p of pre-CuZn-CuNW

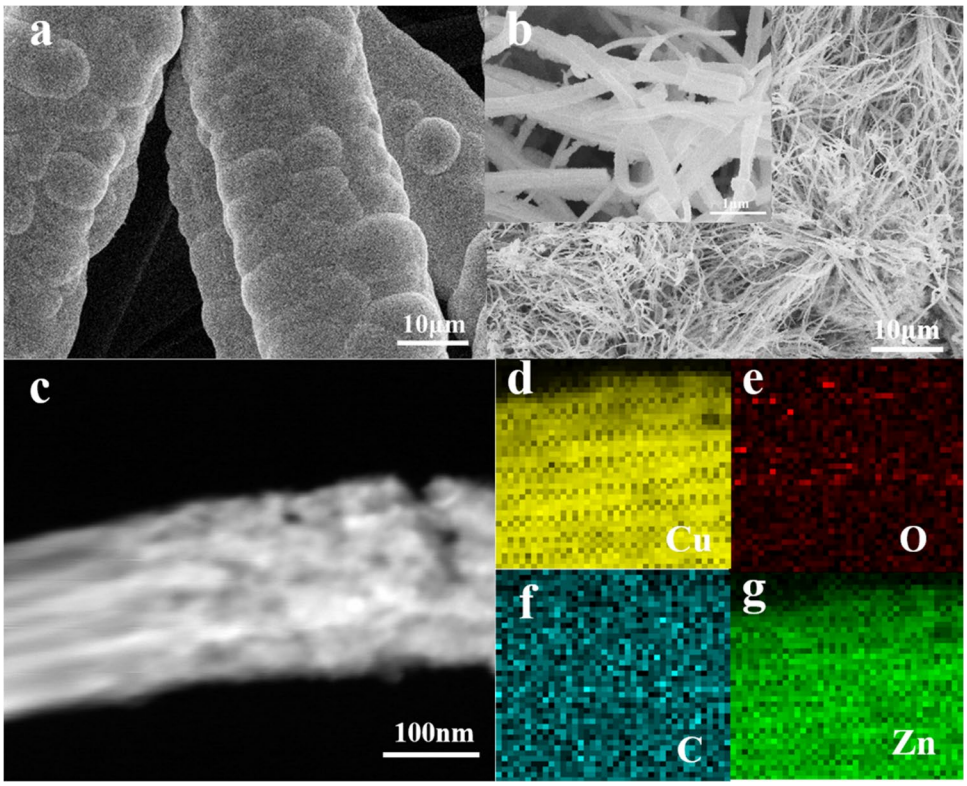

Fig. 3 SEM images of **a** CuZn alloy and **b** pre-CuZn-CuNW, **c**TEM image of pre-CuZn-CuNW, and EDS elemental maps of pre-CuZn-CuNW for **d** copper, **e** oxygen, **f** carbon, and **g** zinc, respectively

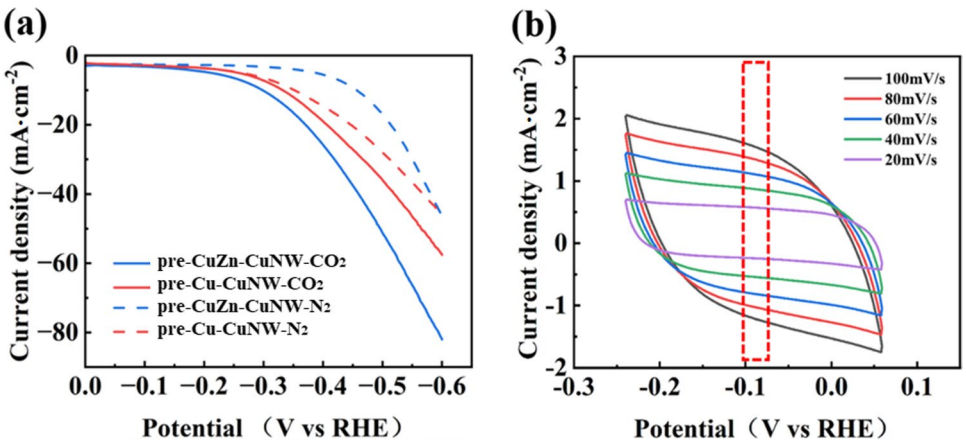

Fig. 4 **a** LSV of copper nanowires in 1 M KOH saturated N_2 or CO_2 at 20 mV•s^{-1} using a flow cell and **b** CV of pre-CuZn-CuNW at different scan rates ranging from 20 to 100 mV•s^{-1} in 0.1 M $KClO_4$ using a H-type cell

Catalytic CO_2RR performance of copper nanowires derived from CuZn alloy

Compared with Cu, CuZn alloy, and pre-Cu-CuNW, pre-CuZn-CuNW shows the best catalytic CO_2RR performance. Their electrochemical testing curves are shown in Figs. 4, S5, and S6. LSV curves were carried out in 1 M KOH saturated CO_2 or N_2. As Figs. 4a and S5a show, the current density at a certain potential of pre-CuZn-CuNW for the reduction of CO_2 is the highest in the potential range of 0 to − 0.6 V, which shows that the pre-CuZn-CuNW has the best catalytic activity for CO_2RR. Pre-CuZn-CuNW exhibits the largest active specific surface area for electrocatalytic reduction of CO_2. For calculating the C_{dl} and ECSA, CV curves were tested at various scan rates. According to Figs. 4b, S5b-d, S6a and b, and S7a, the values of C_{dl} and ECSA of four catalysts are listed in Table 1. For 1 cm^2

Table 1 C_{dl} and ECSA of various catalysts

Catalysts	C_{dl} (mF cm^{-2})	ECSA (cm^2)
Cu	11.86	0.20
CuZn alloy	10.83	0.18
Pre-Cu-CuNW	19.73	0.33
Pre-CuZn-CuNW	24.28	0.41

samples in geometry, the ECSA of Cu, CuZn alloy, pre-Cu-CuNW, and pre-CuZn-CuNW are 0.20, 0.18, 0.33, and 0.41 cm^2, respectively. Therefore, the pre-CuZn-CuNW has the largest ECSA among the above catalysts.

The pre-CuZn-CuNW also shows excellent selectivity for C_2H_4 and high current density. As seen from Fig. 5a, the FE for C_2H_4 production of the pre-CuZn-CuNW is 46% at − 0.8 V, while the FE for C_2H_4 production of other catalysts is less than 30% in potential range of − 0.4 to − 1.0 V as shown in Figs. S5e, S5g, and S6c. Furthermore, the pre-CuZn-CuNW exhibits good stability under − 0.8 V for 24 h. It can be seen from Fig. 5b that the total geometric current density of the catalyst pre-CuZn-CuNW is fluctuate and maintained stably at 170 ± 20 mA·cm^{-2} at − 0.8 V. The FEs for C_2H_4 production of the pre-CuZn-CuNW were taken every 6 h, which were stabilized above 50% and better than the initial. The pre-CuZn-CuNW exhibits a competitive selectivity and stability for C_2H_4 in this work compared with other similar research as Table 2 shown [26–33]. By calculating with ECSA, the partial normalized current densities for C_2H_4 production at − 0.8 V of Cu, CuZn, pre-Cu-CuNW, and pre-CuZn-CuNW are 49, 34, 97, and 183 mA·cm^{-2}, respectively. It indicates that the pre-CuZn-CuNW has the best intrinsic activity for C_2H_4 production among these catalysts.

It is worth noting that the order of the catalytic performance for the catalysts from high to low is pre-CuZn-CuNW, pre-Cu-CuNW, Cu, and CuZn alloy. The nanowire catalyst derived from the CuZn alloy has the best activity and selectivity for C_2H_4 production, but the catalytic performance of the CuZn alloy is lower than that of the Cu. To illustrate the role of Zn during the preparation of the catalysts is interesting, compared with the Cu, the CuZn alloy exhibits a lower activity and selectivity for C_2H_4 in the CO_2RR test while the partial geometric current density for C_2H_4 production was 6.2 mA·cm^{-2} and FE for C_2H_4 production was 17% at − 0.8 V (Fig. S5g). Because of the addition of zinc, the CuZn alloy has a smaller ECSA than that of the Cu catalyst. It indicates that the zinc element is useless for promoting the performance of the catalyst during the CO_2RR. However, for the nanowires derived from the CuZn alloy, the chemical dezincification in the process of nanowires growth not only results in a special structure of pre-CuZn-CuNW with a larger surface area than that of pre-Cu-CuNW but also provides higher intrinsic activity for C_2H_4 because of more CO* dimerization [34].

Table 2 Stability of electrochemical CO_2 reduction to C_2H_4

Catalysts	Stability (h)	FE_{C2H4} (%)
Cu_I [26]	22.5	35
Cu NDs [27]	7	22.3
44 nm Cu nanocube [28]	1	41
Cu-on-Cu3N [29]	15	39 ± 2
F-Cu [30]	40	65.2
3D porpus CuO [31]	2	39.3
CSNP [32]	20	48.7
HPR-Cu [33]	40	38.1

Conclusions

Binder-free copper-based catalyst pre-CuZn-CuNW was loaded on carbon paper by electrodeposition, wet chemical oxidation, annealing, and electrochemical reduction. The pre-CuZn-CuNW has abundant nanowires in diameter of around 170 nm and presents a radial structure. The Zn atomic content in CuZn alloy is 2.99%, while in the pre-CuZn-CuNW, it is 0.52%. The vacancies were left in nanowires by the entry and exit of zinc atoms in Cu crystal lattice during CuZn codeposition and chemical dezincification process, which cause larger electrochemical active surface area and higher intrinsic activity of the pre-CuZn-CuNW. Compared with Cu, CuZn alloy, and pre-Cu-CuNW, pre-CuZn-CuNW exhibits the highest activity, selectivity, and stability for ethylene production. In a flow cell, at − 0.8 V (vs RHE), the FE for ethylene production of pre-CuZn-CuNW is over 46% for 24 h under a total geometric current density of 170 ± 20 mA•cm^{-2}, which is competitive among similar

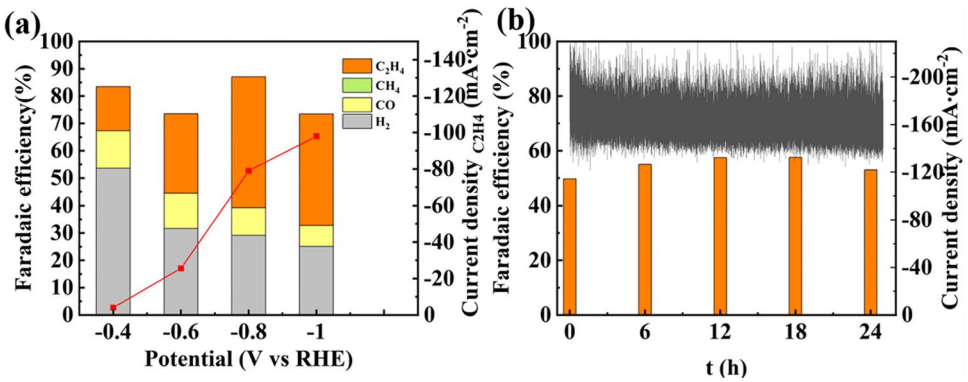

Fig. 5 **a** FEs for gas products and geometric current density for ethylene production of pre-CuZn-CuNW under different potential in CO_2RR, **b** stability testing of pre-CuZn-CuNW at − 0.8 V (vs RHE) in 1 M KOH using a flow cell while the black curve corresponds to the CO_2RR geometric current density and the orange histograms are the FEs for ethylene production at different sampling time

research and provides a possibility for subsequent industrial applications. In the future work, the proposed reaction mechanism could be verified by more experimental and theoretical methods. In addition, the selectivity and stability of the copper nanowires catalyst may be enhanced by adjusting the ratio of Cu to Zn in the electrodeposition system.

Supplementary Information The online version contains supplementary material available at https://doi.org/10.1007/s11581-022-04723-z.

Declarations

Conflict of interest The authors declare no competing interests.

References

1. Zhu DD, Liu JL, Qiao SZ (2016) Recent advances in inorganic heterogeneous electrocatalysts for reduction of carbon dioxide. Adv Mater 28:3423–3452
2. Clark EL, Hahn C, Jaramillo TF, Bell AT (2017) Electrochemical CO_2 reduction over compressively strained CuAg surface alloys with enhanced multi-carbon oxygenate selectivity. J Am Chem Soc 139:15848–15857
3. Gao D, Zhang Y, Zhou Z, Cai F, Zhao X, Huang W, Li Y, Zhu J, Liu P, Yang F, Wang G, Bao X (2017) Enhancing CO_2 electroreduction with the metal-oxide interface. J Am Chem Soc 139:5652–5655
4. Ju W, Bagger A, Hao GP, Varela AS, Sinev I, Bon V, Roldan Cuenya B, Kaskel S, Rossmeisl J, Strasser P (2017) Understanding activity and selectivity of metal-nitrogen-doped carbon catalysts for electrochemical reduction of CO_2. Nat Commun 8:944
5. Weekes DM, Salvatore DA, Reyes A, Huang A, Berlinguette CP (2018) Electrolytic CO_2 reduction in a flow cell. Acc Chem Res 51:910–918
6. Mistry H, Varela AS, Bonifacio CS, Zegkinoglou I, Sinev I, Choi YW, Kisslinger K, Stach EA, Yang JC, Strasser P, Cuenya BR (2016) Highly selective plasma-activated copper catalysts for carbon dioxide reduction to ethylene. Nat Commun 7:12123
7. Bertheussen E, Verdaguer-Casadevall A, Ravasio D, Montoya JH, Trimarco DB, Roy C, Meier S, Wendland J, Norskov JK, Stephens IE, Chorkendorff I (2016) Acetaldehyde as an intermediate in the electroreduction of carbon monoxide to ethanol on oxide-derived copper. Angew Chem Int Ed Engl 55:1450–1454
8. Roberts FS, Kuhl KP, Nilsson A (2016) Electroreduction of carbon monoxide over a copper nanocube catalyst: surface structure and ph dependence on selectivity. ChemCatChem 8:1119–1124
9. Dutta A, Rahaman M, Luedi NC, Mohos M, Broekmann P (2016) Morphology matters: tuning the product distribution of CO_2 electroreduction on oxide-derived Cu foam catalysts. ACS Catal 6:3804–3814
10. Yang KD, Ko WR, Lee JH, Kim SJ, Lee H, Lee MH, Nam KT (2017) Morphology-directed selective production of ethylene or ethane from CO_2 on a Cu mesopore electrode. Angew Chem Int Ed Engl 56:796–800
11. Ma M, Djanashvili K, Smith WA (2016) Controllable hydrocarbon formation from the electrochemical reduction of CO_2 over Cu nanowire arrays. Angew Chem Int Ed Engl 55:6680–6684
12. Feng X, Jiang K, Fan S, Kanan MW (2016) A direct grain-boundary-activity correlation for CO electroreduction on Cu nanoparticles. ACS Cent Sci 2:169–174
13. Li CW, Ciston J, Kanan MW (2014) Electroreduction of carbon monoxide to liquid fuel on oxide-derived nanocrystalline copper. Nature 508:504–507
14. Gupta N, Gattrell M, MacDougall B (2005) Calculation for the cathode surface concentrations in the electrochemical reduction of CO_2 in $KHCO_3$ solutions. J Appl Electrochem 36:161–172
15. Varela AS, Kroschel M, Reier T, Strasser P (2016) Controlling the selectivity of CO_2 electroreduction on copper: the effect of the electrolyte concentration and the importance of the local pH. Catal Today 260:8–13
16. Schouten KJP, Pérez Gallent E, Koper MTM (2014) The influence of pH on the reduction of CO and CO_2 to hydrocarbons on copper electrodes. J Electroanal Chem 716:53–57
17. Lum Y, Yue B, Lobaccaro P, Bell AT, Ager JW (2017) Optimizing C-C coupling on oxide-derived copper catalysts for electrochemical CO_2 reduction. J Phys Chem C 121:14191–14203
18. Raciti D, Livi KJ, Wang C (2015) Highly dense Cu nanowires for low-overpotential CO_2 reduction. Nano Lett 15:6829–6835
19. Wu JJ, Sharma PP, Harris BH, Zhou XD (2014) Electrochemical reduction of carbon dioxide: IV dependence of the Faradaic efficiency and current density on the microstructure and thickness of tin electrode. J Power Sources 258:189–194
20. Gonçalves MR, Gomes A, Condeço J, Fernandes TRC, Pardal T, Sequeira CAC, Branco JB (2013) Electrochemical conversion of CO_2 to C_2 hydrocarbons using different ex situ copper electrodeposits. Electrochim Acta 102:388–392
21. Chen X, Henckel DA, Nwabara UO, Li Y, Frenkel AI, Fister TT, Kenis PJA, Gewirth AA (2019) Controlling speciation during CO_2 reduction on Cu-alloy electrodes. ACS Catal 10:672–682
22. Feng R, Zhu Q, Chu M, Jia S, Zhai J, Wu H, Wu P, Han B (2020) Electrodeposited Cu–Pd bimetallic catalysts for the selective electroreduction of CO_2 to ethylene. Green Chem 22:7560–7565
23. Wang S, Zhang D, Li B, Zhang C, Du Z, Yin H, Bi X, Yang S (2018) Ultrastable in-plane 1T–2H MoS2 heterostructures for enhanced hydrogen evolution reaction. Adv Energy Mater 8:1801345–1801351
24. Peng Y, Wu T, Sun L, Nsanzimana JMV, Fisher AC, Wang X (2017) Selective electrochemical reduction of CO_2 to ethylene on nanopores-modified copper electrodes in aqueous solution. ACS Appl Mater Interfaces 9:32782–32789
25. Shao X, Zhang Q, Zhang X, Yi J, Liu Y, Zhang J (2020) Nanoporous structured Sn-MWCNT/Cu electrodes fabricated by electrodeposition–chemical dezincification for catalytic CO_2 reduction. Int J Energy Res 45:6273–6284
26. Gao D, Sinev I, Scholten F, Aran-Ais RM, Divins NJ, Kvashnina K, Timoshenko J, Roldan Cuenya B (2019) Selective CO_2 electroreduction to ethylene and multicarbon alcohols via electrolyte-driven nanostructuring. Angew Chem Int Ed Engl 58:17047–17053
27. Wu M, Zhu C, Wang K, Li G, Dong X, Song Y, Xue J, Chen W, Wei W, Sun Y (2020) Promotion of CO_2 electrochemical reduction via cu nanodendrites. ACS Appl Mater Interfaces 12:11562–11569
28. Loiudice A, Lobaccaro P, Kamali EA, Thao T, Huang BH, Ager JW, Buonsanti R (2016) Tailoring copper nanocrystals towards C_2 products in electrochemical CO_2 reduction. Angew Chem Int Ed Engl 55:5789–5792
29. Liang ZQ, Zhuang TT, Seifitokaldani A, Li J, Huang CW, Tan CS, Li Y, De Luna P, Dinh CT, Hu Y, Xiao Q, Hsieh PL, Wang Y, Li F, Quintero-Bermudez R, Zhou Y, Chen P, Pang Y, Lo SC, Chen LJ, Tan H, Xu Z, Zhao S, Sinton D, Sargent EH (2018) Copper-on-nitride enhances the stable electrosynthesis of multi-carbon products from CO_2. Nat Commun 9:3828

30. Ma W, Xie S, Liu T, Fan Q, Ye J, Sun F, Jiang Z, Zhang Q, Cheng J, Wang Y (2020) Electrocatalytic reduction of CO_2 to ethylene and ethanol through hydrogen-assisted C-C coupling over fluorine-modified copper. Nat Catal 3:478–487
31. Lv JJ, Jouny M, Luc W, Zhu W, Zhu JJ, Jiao F (2018) A highly porous copper electrocatalyst for carbon dioxide reduction. Adv Mater 30:e1803111
32. Lee SY, Chae SY, Jung H, Lee CW, Nguyen DLT, Oh H-S, Min BK, Hwang YJ (2020) Controlling the C_{2+} product selectivity of electrochemical CO_2 reduction on an electrosprayed Cu catalyst. J Mater Chem A 8:6210–6218
33. Lee SY, Jung H, Kim NK, Oh HS, Min BK, Hwang YJ (2018) Mixed copper states in anodized Cu electrocatalyst for stable and selective ethylene production from CO_2 reduction. J Am Chem Soc 140:8681–8689
34. Zheng Y, Vasileff A, Zhou X, Jiao Y, Jaroniec M, Qiao SZ (2019) Understanding the roadmap for electrochemical reduction of CO_2 to multi-carbon oxygenates and hydrocarbons on copper-based catalysts. J Am Chem Soc 141:7646–7659